Analytical Methods

Deutsche Ausgabe: DOI: 10.1002/ange.201908600
Internationale Ausgabe: DOI: 10.1002/anie.201908600

Chemically Induced Sintering of Nanoparticles

*Zheng Li and Kenneth S. Suslick**

Abstract: *We have observed solid-state growth of pre-existing silver nanoparticles (AgNPs) upon exposure to trace (ppb) concentrations of reactive gases at room temperature. The consequent change in localized surface plasmon resonances alters the visible absorbance of dried, printed sensor spots made from inks of 10 nm-AgNPs and provides a novel mechanism for trace detection and dosimetry of reactive gases. Colorimetric sensor arrays based on these AgNP inks offer dosimetric identification of acidic and oxidizing gases and other reactive vapors with limits of detection below ppb levels for 1 h exposures. For an array of AgNP inks with various capping agents, a unique color response pattern is observed for each specific analyte. Excellent discrimination among 11 reactive gases was demonstrated using standard chemometric methods. The chemically induced sintering of NPs paves the way for novel solid-state sensors for the ultrasensitive detection of reactive gases and their application to the monitoring of trace airborne pollutants.*

Sintering of nanometer-sized noble metal particles accounts for many important chemical phenomena in industrial production, such as inkjet printing of electronic circuits[1–3] and deactivation of nanostructured heterogeneous catalysts.[4–8] Nanoparticles are prone to sinter or coalesce into larger particles even under mild conditions owing to their large surface-to-volume ratio and consequent high surface energy. The growth of nanoparticles is a complex physical and chemical process governed by multiple factors, including particle size, metal type, temperature, chemical environment, and nature of the substrate. Despite extensive research on sintering over the past decade, the detailed mechanisms of sintering, in particular chemical circumstances (e.g., in oxidative vs. reductive atmospheres), are still far from fully understood.[9,10] A deep understanding of the mechanisms of nanoparticle sintering (and the consequent changes in plasmonic behavior) in the presence of reactive gases will permit the development of new applications of this interesting chemical process in areas ranging from microelectronics fabrication, 3D printing, and heterogeneous catalysis to applications in chemical sensing and environmental monitoring[11] and even facial recognition.[12]

Two generic mechanisms are usually proposed in a nanoparticle sintering[9,10,13,14] process: 1) Particle diffusion, collision, and coalescence (e.g., cold-welding) between two nanoparticles over the support, and 2) atomic migration from one nanoparticle to another, either by dissolution/precipitation in solution or by gas-phase volatile transport from complex formation and decomposition (e.g., Ostwald ripening).

Non-sintering aggregation of metal nanoparticles (particularly gold or silver) constitutes an important class of colorimetric and fluorometric sensors that are extensively employed for the detection of biological macromolecular analytes.[15–21] These sensors rely on changes in localized surface plasmon resonance (LSPR) for the detection of biomacromolecules by nanoparticle aggregation induced by biomolecules binding to nanoparticles (e.g., through surface-bound antibodies). Similar AgNPs have also found broad applications in environmental monitoring, pharmaceutics, food safety, and security screening.[22–24] Very few attempts, however, have been made to detect small molecules in the gas phase using AgNPs, with the notable exception of the detection of NO_2,[25] H_2S,[26] and NH_3[27] with Ag nanostructures or nanofilms.

Inspired by the phenomenon of nanocatalyst sintering that occurs under reactive conditions during heterogeneous catalytic processes, we have discovered the solid-state growth of pre-existing silver nanoparticles (AgNPs) upon exposure to only trace concentrations of reactive gases at room temperature. Such chemically induced sintering of nanoparticles and the consequent change in localized surface plasmon resonances alters the visible absorbance of the AgNPs and provides a novel potential mechanism for the trace detection and dosimetry of reactive gases. We have created a solid-state, nanoparticle-based disposable colorimetric sensor array (CSA) made from printable inks of 10 nm AgNPs with several different capping agents (detailed in Supporting Information) in hydrocarbon solutions (Figure 1). Changes in the plasmonic absorbance of visible light owing to chemically induced sintering are induced by trace levels of reactive gases. The AgNP CSA offers ultrasensitive dosimetric identification of acidic and oxidizing gases and other reactive vapors; the limits of detection are below ppb levels for 1 h exposures. The use of the sensor array also permits differentiation among and quantitative identification of 11 common reactive gases relevant to atmospheric pollution and environmental monitoring.

The as-synthesized AgNPs have an average diameter of circa 10 nm; the dodecanethiol-capped AgNP gives the most monodispersed nanocrystals (Supporting Information, Figure S1). The FTIR spectra are dominated by the capping agents' vibrational bands (Figure S2). Powder X-ray diffraction patterns demonstrate that all three AgNPs crystallize in the expected face-centred cubic (fcc) phase of Ag (Figure S3). The surface chemistry of the capped AgNPs was further validated by XPS, which reveals the presence of N atoms on the surface of AgNP-A and S atoms on AgNP-B and AgNP-C (Figure S4).

[*] Dr. Z. Li, Prof. Dr. K. S. Suslick
Department of Chemistry, University of Illinois at Urbana-Champaign
600 S Matthews Ave, Urbana, IL 61801 (USA)
E-mail: ksuslick@illinois.edu

Supporting information and the ORCID identification number(s) for the author(s) of this article can be found under: https://doi.org/10.1002/anie.201908600.

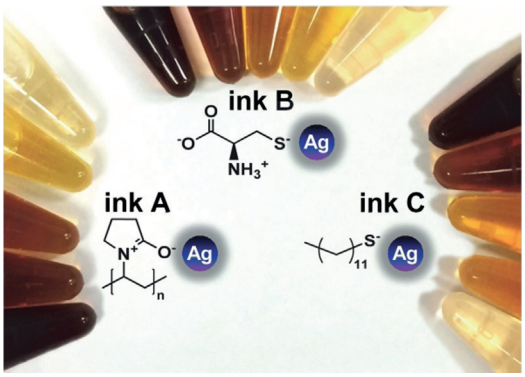

Figure 1. Silver nanoparticle (AgNP) inks. Photographs of three AgNP inks used as colorimetric sensors at 0.51, 0.38, 0.33, 0.29, and 0.26 mM total Ag concentration.

AgNP sintering occurs upon exposure to reactive gases but not to N_2 or other unreactive vapours, even for dry, printed spots of nanosilver inks, as seen in TEM images (Figure 2). The primary mechanism for this sintering during reactive gas exposure is the particle diffusion and cold-welding of intact nanoparticles, not gas-phase transport and Ostwald ripening. Nanoparticles remain intact but grow together and fuse at points of contact, as seen in Figure 2. Even at room temperature in the presence of trace levels of reactive gases, individual nanoparticles deposited on innocent substrates (e.g., polypropylene membranes or amorphous carbon TEM grids) have sufficient mobility to allow migration of the nanoparticles, cold-welding fusion with neighbouring nanoparticles, and eventually formation of extended aggregates.

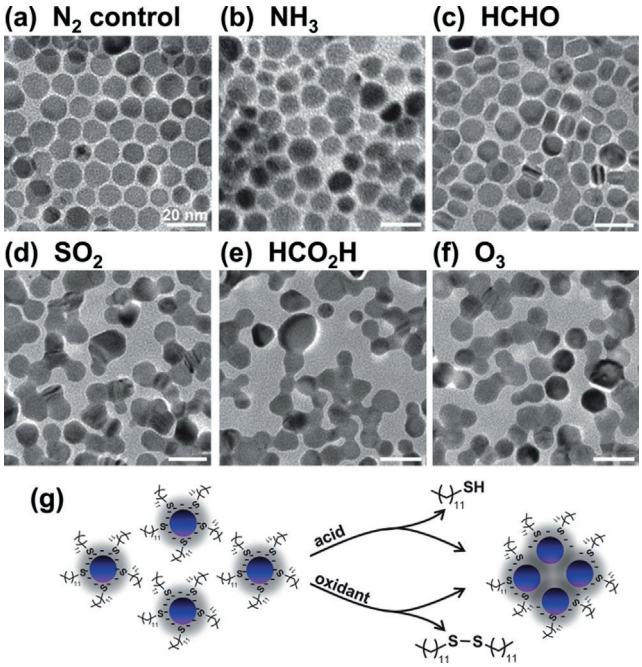

Figure 2. The primary mechanism for AgNP colorimetric sensing is sintering of NPs upon exposure to analytes. Transmission electron micrographs of drop-cast AgNP inks dried and then exposed for 10 min to a) N_2 (control), and to 1 ppm of b) NH_3, c) HCHO, d) SO_2, e) HCO_2H, and f) O_3. g) Proposed agglomeration mechanism in the presence of acids or oxidants, which initiate removal of thiol capping agents and consequent particle sintering; further details for PVP-AgNPs are given in Scheme S1. The specific AgNP ink in (a–f) was dodecanethiol-capped AgNPs at 0.29 mM total Ag concentration in toluene, the same as spot 14 in the sensor array described in Figure 3. All micrographs are the same magnification; scale bars = 20 nm.

The rate and extent of sintering depends on the reactivity of the specific gas exposure. As shown in Figure 2a–f, substantial particle sintering only occurs in the presence of relatively strong acids or oxidants (e.g., SO_2, HCO_2H, and O_3). Upon exposure to these reactive gases, loss of surface capping ligands is likely due to their protonation or oxidation; if capping agents are partially stripped from the core of AgNPs, sintering is much more likely to occur even in the solid state,[13] as has also been reported for silver colloids in acidic or oxidizing solutions.[28,29]

With acidic gases, protonation of the capping ligands will result in their deligation from the AgNP surface. The resulting agglomeration is relatively rapid, even in the dried sensor spots; the progression of agglomeration is shown over the course of 1 h in Figure S5. The response to acidic analytes should depend on the pK_a of the capping ligands; the larger the pK_a, the more easily protonated. Indeed, at least qualitatively for weakly acidic analytes (e.g., 1 ppm acetic acid in Figure 2), ink C is more responsive than ink B than ink A, which follows the trend of the capping agents pK_a values (dodecanethiol, cys, and PVP have pK_a values of 11, 8.2, and 3.6, respectively).

With oxidizing gases, oxidation of the capping agents is likely to generate products less able to bind to the AgNP, such as the probable disulfide products from cys- and dodecanethiol-capped AgNPs, or a possible poly(vinyl succinimide) (PVS) product[30] from PVP-capped AgNPs (Figure 2g), which again leads to agglomeration and change in colour (Figure S6a). In the case of H_2S as an analyte, formation of Ag_2S is likely, which causes the printed sensor spot to turn black, as observed (Figure S6b). For the exposure to less reactive gases (i.e., N_2, CO, NH_3, HCHO, and toluene vapour), little or no changes in nanoparticle morphology are observed (Figure 2).

Upon exposure to reactive gases, changes in the UV/Vis absorption plasmon bands of AgNP inks (430 to 460 nm, responsible for their characteristic yellow to brown colours, Figure 1 and Figures S7 and S8) are observed. Given the sintering of AgNPs that we observe upon exposure to these gases and the known particle size dependence of the plasmon bands,[9,31] it should be no surprise that we also observe colour changes in exposed spots printed from the AgNP inks (Figure 3 and Figures S6, S8, and S9). For the exposure to less reactive gas analytes (i.e., CO, NH_3, and toluene), which do not produce substantial changes in the AgNP morphology, only small colour changes were observed from the array.

Discrimination among reactive gases is achieved by using a AgNP-based colorimetric sensor array (CSA). Given the irreversible nature of chemically induced sintering of AgNPs, it did not escape our attention that these might serve as dosimetric chemical sensors for trace detection of reactive gases. CSAs have been developed as an inexpensive opto-electronic nose[32–35] for the detection and identification of both individual compounds[36,37] and highly similar complex mixtures,[38–42] generally with limits of detection (LODs) at

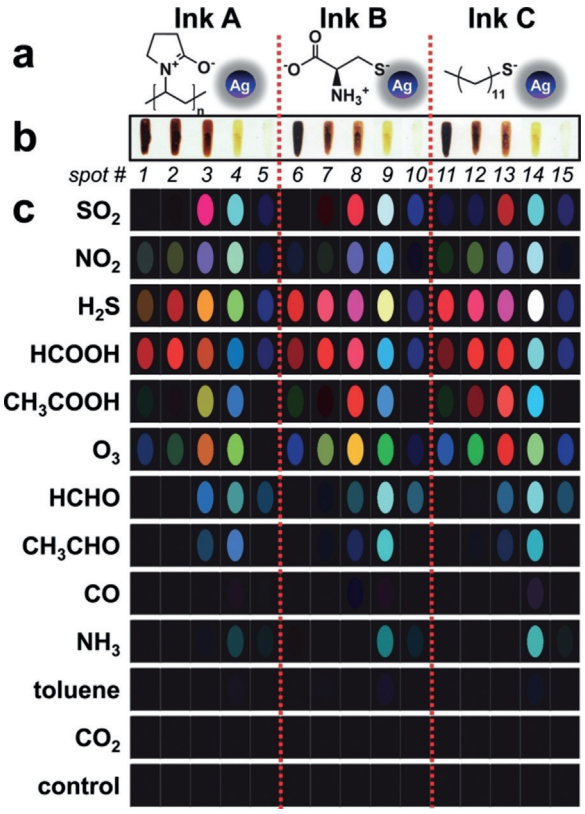

Figure 3. Response of a AgNP colorimetric sensor array to 11 different gases. a) Formulations of the AgNP inks. b) Printed bars of the 15 different inks printed on polypropylene membrane. c) Difference maps of the colour changes (RGB values) of the array to 11 gas species at 1 ppm, CO_2 at 8000 ppm, and a clean-air control, all at 50% relative humidity. For visualization, the colour range is expanded from 3 to 8 bits per colour (i.e., the RGB colour range of 3–10 was expanded to 0–255).

ppm to tens of ppb levels and mostly in vapour phases. CSAs have relied on chemoresponsive dyes with a diverse range of dye–analyte interactions including Brønsted and Lewis acid–base, vapochromic, and redox responses. Most of these interactions, however, are mostly reversible and do not provide the capability of cumulative (i.e., dosimetric) monitoring of analytes.

To generate a AgNP-based CSA, AgNP inks (Figure 3a) were diluted to a series of concentrations and printed on hydrophobic polypropylene membranes as bar-shaped sensor elements ("spots") with distinctive colours (Figure 3b) after solvent evaporation. Printing the hydrophobic inks on hydrophobic membranes minimizes interference from changes in humidity and alleviates chemical interactions with hydrophilic species during long-term storage (shelf-life of circa 2 months under N_2 in aluminized Mylar bags[36,38]). The colour changes (Figure 3c) of the printed AgNP spots in the sensor array (i.e., changes in the RGB values) upon analyte exposure come from red-shifts of the plasmon bands, as seen in the diffuse reflectance spectra of printed AgNP sensor spots (Figure S9) and the colour difference profiles (Figures 3 and Figures S6 and S8). These red-shifts are primarily extrinsic size effects originating from AgNP aggregation in the printed spots (as previously discussed).

As shown in Figure 3, the pattern of the colorimetric response of the AgNP sensor array provides a facile means to differentiate one analyte from another, even by eye. Readily distinguishable patterns for each of the 11 reactive gases are seen. The intensity of the colour change of any given sensor spot induced by nanoparticle sintering is dependent on the chemical properties of the analytes, the initial ink concentration, and the choice of capping agent used.

To evaluate more quantitatively the ability of the array to discriminate among types of gas pollutants, hierarchical cluster analysis (HCA) was employed (Figure S10); the HCA dendrogram of 11 pollutants at 1 ppm concentration and a control (clean air) in quintuplicate trials shows excellent discrimination among analytes. CO and the control are relatively close in clustering, reflecting the lack of significant sintering in both cases. The clusters representing toluene and NH_3 are also relatively close, largely owing to the weak and non-specific interactions involved for those two analytes.

Given sufficient exposure time, the limits of detection (LODs) for cumulative, dosimetric sensors can be very low. For ultrasensitive detection of environmentally relevant pollutants, time is often not of the essence, and it is the response to gas analytes during long-term exposure at very low concentrations that is most important. For example, the permissible exposure limit (PEL) established by NIOSH is based on a time-weighted average over 8 h (Table S1). Another example is the recommended level of exposure to airborne pollutants for cultural heritage objects (e.g., artwork), which are often in the low ppb regime (Table S1).[43,44]

Prior CSAs are too reversible to be used for cumulative ultra-sensitive detection; consequently, with prior arrays, sensitivity does not improve with increased exposure time, and previous arrays must be imaged in real-time. In addition, prior CSAs showed eventual response to CO_2 (an acidic gas present at ca. 400 ppm in air), which limited their usefulness for long-term monitoring of pollutants.

The AgNP sensor array's LODs for critical museum pollutants are listed in Table S1 and compared to the PELs and to the suggested exposure limits for cultural heritage collection materials.[43] The AgNP sensor arrays are dosimetric (i.e., cumulative) and generally show sub-ppb LODs for one-hour passive exposures (i.e., ambient air motion only), as illustrated in Figure S11; these analyte sensitivities are well below their respective PELs (typically by more than a thousand-fold) and generally even below the extremely stringent exposure limits suggested for cultural heritage materials. We note that these LODs can be pushed even lower simply by extending the total exposure time or by active (i.e., pumped gas flow) sampling. For comparison, our observed LODs are one to two orders of magnitude more sensitive than commercial exposure indicators (e.g., Draeger tubes, Table S2) that are used in museum environments[43,44] and considerably faster than traditional qualitative Oddy tests (which often require a week).[45]

Cumulative sensor responses to changes in humidity or to the constant background concentration of CO_2 in air are particularly problematic for pollutant monitoring. The AgNP sensor array is impressively unaffected by these common potential interferents. Specifically, the sensor array response to pollutants is unaffected over a wide range of relative

humidity levels, i.e., 5 to 95% RH (Figure S12). Importantly, the array is also particularly insensitive to CO_2 in air, which is a problematic cumulative interferent, particularly for pH indicating dyes as sensors.[46] For AgNP sensors, however, even at 20-fold its ambient level (i.e., 8000 ppm), CO_2 shows no colorimetric response (Figure 3).

The remarkable observation of nanoparticle sintering in printed arrays opens a new class of solid-state dosimetric sensors for ultrasensitive detection of reactive gases. The use of a disposable array of AgNP colorimetric sensors with different capping groups provides ready analysis by digital imaging and permits identification and sub-ppb detection of classes of pollutants relevant to the protection of cultural heritage objects and museum environmental monitoring.

Acknowledgements

Z.L. acknowledges postdoctoral financial support from the Procter and Gamble Foundation. This work was carried out in part in the Materials Research Laboratory Central Facilities at UIUC.

Conflict of interest

The authors declare no conflict of interest.

Keywords: colorimetric sensor arrays · gas–solid reaction · nanoparticle sensors · sintering · ultrasensitive dosimetry

How to cite: *Angew. Chem. Int. Ed.* **2019**, *58*, 14193–14196
Angew. Chem. **2019**, *131*, 14331–14334

[1] B. Y. Ahn, E. B. Duoss, M. J. Motala, X. Guo, S.-I. Park, Y. Xiong, J. Yoon, R. G. Nuzzo, J. A. Rogers, J. A. Lewis, *Science* **2009**, *323*, 1590–1593.
[2] J. A. Rogers, T. Someya, Y. Huang, *Science* **2010**, *327*, 1603–1607.
[3] W. Wu, *Nanoscale* **2017**, *9*, 7342–7372.
[4] S. Zhang, L. Nguyen, Y. Zhu, S. Zhan, C.-K. Tsung, F. Tao, *Acc. Chem. Res.* **2013**, *46*, 1731–1739.
[5] U. Hejral, P. Müller, O. Balmes, D. Pontoni, A. Stierle, *Nat. Commun.* **2016**, *7*, 10964.
[6] P. Tabib Zadeh Adibi, T. Pingel, E. Olsson, H. Grönbeck, C. Langhammer, *ACS Nano* **2016**, *10*, 5063–5069.
[7] K. Manthiram, Y. Surendranath, A. P. Alivisatos, *J. Am. Chem. Soc.* **2014**, *136*, 7237–7240.
[8] L. L. Chng, N. Erathodiyil, J. Y. Ying, *Acc. Chem. Res.* **2013**, *46*, 1825–1837.
[9] T. W. Hansen, A. T. DeLaRiva, S. R. Challa, A. K. Datye, *Acc. Chem. Res.* **2013**, *46*, 1720–1730.
[10] C. T. Campbell, *Acc. Chem. Res.* **2013**, *46*, 1712–1719.
[11] Y. Su, G. Xie, H. Tai, S. Li, B. Yang, S. Wang, Q. Zhang, H. Du, H. Zhang, X. Du, Y. Jiang, *Nano Energy* **2018**, *47*, 316–324.
[12] M. Su, F. Li, S. Chen, Z. Huang, M. Qin, W. Li, X. Zhang, Y. Song, *Adv. Mater.* **2016**, *28*, 1369–1374.
[13] D. V. Wagle, G. A. Baker, *Mater. Horiz.* **2015**, *2*, 157–167.
[14] S. E. Wanke, P. C. Flynn, *Catal. Rev.* **1975**, *12*, 93–135.
[15] N. D. B. Le, G. Yesilbag Tonga, R. Mout, S.-T. Kim, M. E. Wille, S. Rana, K. A. Dunphy, D. J. Jerry, M. Yazdani, R. Ramanathan, C. M. Rotello, V. M. Rotello, *J. Am. Chem. Soc.* **2017**, *139*, 8008–8012.
[16] G. Chen, I. Roy, C. Yang, P. N. Prasad, *Chem. Rev.* **2016**, *116*, 2826–2885.
[17] M. Sabela, S. Balme, M. Bechelany, J.-M. Janot, K. Bisetty, *Adv. Eng. Mater.* **2017**, *19*, 1700270.
[18] H. Wei, S. M. Hossein Abtahi, P. J. Vikesland, *Environ. Sci. Nano* **2015**, *2*, 120–135.
[19] J. D. Padmos, M. L. Personick, Q. Tang, P. N. Duchesne, D.-e. Jiang, C. A. Mirkin, P. Zhang, *Nat. Commun.* **2015**, *6*, 7664.
[20] K. L. Young, M. B. Ross, M. G. Blaber, M. Rycenga, M. R. Jones, C. Zhang, A. J. Senesi, B. Lee, G. C. Schatz, C. A. Mirkin, *Adv. Mater.* **2014**, *26*, 653–659.
[21] M. Avella, M. Cocca, M. E. Errico, G. Gentile, in *Nanotechnological Basis for Advanced Sensors* (Eds.: J. P. Reithmaier, et al.), Springer, Dordrecht, **2010**, pp. 511–517.
[22] W. Lewandowski, M. Fruhnert, J. Mieczkowski, C. Rockstuhl, E. Górecka, *Nat. Commun.* **2015**, *6*, 6590.
[23] M. Rycenga, C. M. Cobley, J. Zeng, W. Li, C. H. Moran, Q. Zhang, D. Qin, Y. Xia, *Chem. Rev.* **2011**, *111*, 3669–3712.
[24] W. J. Stark, P. R. Stoessel, W. Wohlleben, A. Hafner, *Chem. Soc. Rev.* **2015**, *44*, 5793–5805.
[25] Q. Zhang, G. Xie, M. Xu, Y. Su, H. Tai, H. Du, Y. Jiang, *Sens. Actuators B* **2018**, *259*, 269–281.
[26] R. Chen, H. R. Morris, P. M. Whitmore, *Sens. Actuators B* **2013**, *186*, 431–438.
[27] D. Rithesh Raj, S. Prasanth, T. V. Vineeshkumar, C. Sudarsanakumar, *Opt. Commun.* **2015**, *340*, 86–92.
[28] J. L. Axson, D. I. Stark, A. L. Bondy, S. S. Capracotta, A. D. Maynard, M. A. Philbert, I. L. Bergin, A. P. Ault, *J. Phys. Chem. C* **2015**, *119*, 20632–20641.
[29] O. V. Dement'eva, V. M. Rudoy, *Colloid J.* **2015**, *77*, 276–282.
[30] S. M. Louie, J. M. Gorham, J. Tan, V. A. Hackley, *Environ. Sci. Nano* **2017**, *4*, 1866–1875.
[31] K. B. Mogensen, K. Kneipp, *J. Phys. Chem. C* **2014**, *118*, 28075–28083.
[32] J. R. Askim, M. Mahmoudi, K. S. Suslick, *Chem. Soc. Rev.* **2013**, *42*, 8649–8682.
[33] S. H. Lim, L. Feng, J. W. Kemling, C. J. Musto, K. S. Suslick, *Nat. Chem.* **2009**, *1*, 562–567.
[34] J. R. Askim, K. S. Suslick, *Anal. Chem.* **2015**, *87*, 7810–7816.
[35] N. A. Rakow, K. S. Suslick, *Nature* **2000**, *406*, 710–713.
[36] Z. Li, M. Fang, M. K. LaGasse, J. R. Askim, K. S. Suslick, *Angew. Chem. Int. Ed.* **2017**, *56*, 9860–9863; *Angew. Chem.* **2017**, *129*, 9992–9995.
[37] Z. Li, H. Li, M. K. LaGasse, K. S. Suslick, *Anal. Chem.* **2016**, *88*, 5615–5620.
[38] Z. Li, K. S. Suslick, *ACS Sens.* **2016**, *1*, 1330–1335.
[39] Z. Li, W. P. Bassett, J. R. Askim, K. S. Suslick, *Chem. Commun.* **2015**, *51*, 15312–15315.
[40] J. R. Carey, K. S. Suslick, K. I. Hulkower, J. A. Imlay, K. R. Imlay, C. K. Ingison, J. B. Ponder, A. Sen, A. E. Wittrig, *J. Am. Chem. Soc.* **2011**, *133*, 7571–7576.
[41] B. A. Suslick, L. Feng, K. S. Suslick, *Anal. Chem.* **2010**, *82*, 2067–2073.
[42] M. Qin, Y. Huang, Y. Li, M. Su, B. Chen, H. Sun, P. Yong, C. Ye, F. Li, Y. Song, *Angew. Chem. Int. Ed.* **2016**, *55*, 6911–6914; *Angew. Chem.* **2016**, *128*, 7025–7028.
[43] C. M. Grzywacz, *Monitoring for gaseous pollutants in museum environments*, Getty Publications, Los Angeles, **2006**.
[44] P. B. Hatchfield, *Pollutants in the Museum Environment*, Archetype Publications, London, **2002**.
[45] J. A. Bamberger, *Stud. Conserv.* **2012**, *57*, 187–188.
[46] M. K. LaGasse, K. McCormick, Z. Li, H. Khanjian, M. Schilling, K. S. Suslick, *J. Amer. Inst. Conserv.* **2018**, *57*, 127–140.

Manuscript received: July 10, 2019
Revised manuscript received: July 25, 2019
Accepted manuscript online: August 2, 2019
Version of record online: August 23, 2019

